Journal of Alloys and Compounds 502 (2010) 184–189

Contents lists available at ScienceDirect

Journal of Alloys and Compounds

journal homepage: www.elsevier.com/locate/jallcom

Spectroscopic properties of Pr^{3+}:$Gd_3Ga_5O_{12}$ crystal

Yan Wang[a,b], Jianfu Li[a], Zhenyu You[a], Zhaojie Zhu[a], Chaoyang Tu[a,*]

[a] Key Laboratory of Optoelectronic Materials Chemistry and Physics of CAS, Fujian Institute of Research on the Structure of Matter, Chinese Academy of Sciences, Fuzhou City, Fujian Province, 350002, PR China
[b] Graduate School of Chinese Academy of Sciences, Beijing City, 100039, PR China

ARTICLE INFO

Article history:
Received 8 December 2009
Received in revised form 15 April 2010
Accepted 17 April 2010
Available online 16 May 2010

PACS:
42.70.Hj
78.20.–e

Keywords:
Pr:$Gd_3Ga_5O_{12}$ crystal
J-O theory calculation
Spectroscopic properties

ABSTRACT

The room-temperature absorption spectrum, fluorescence spectra, and fluorescence decay curves of Pr^{3+}-doped $Gd_3Ga_5O_{12}$ single crystal were studied systematically. The standard and modified Judd–Ofelt theories were used to determine the Judd–Ofelt intensity parameters Ω_t ($t = 2, 4, 6$), radiative transition probabilities, radiative lifetimes and branching ratios. The stimulated emission cross-sections and the fluorescence quantum efficiency of the promising laser levels were calculated and discussed. The multi-exponential behavior of the fluorescence decay curve of the $^1D_2 \rightarrow {}^3H_4$ transition was explained by using the Inokuti–Hirayama theory. The obtained spectroscopic results show the potential application of the Pr^{3+}-doped $Gd_3Ga_5O_{12}$ crystal as visible solid-state lasers.

1. Introduction

Among different rare-earth ions, the trivalent praseodymium ion (Pr^{3+}) has been found to be very attractive due to its intricate energy level scheme with various energy gaps. It demonstrates a wide and complex emission spectra extending from ultraviolet (UV) to mid-infrared (MIR) regions. Recently the spectroscopic properties of Pr^{3+} ion have been investigated extensively in various hosts including single crystals [1–3], nanocrystals [4], powders [5–8], glasses [9], etc. When the Pr^{3+} ions are pumped to the closely grouped ^3P_J ($J = 0, 1, 2$) multiplets, several emissions in red ($^3P_0 \rightarrow {}^3F_2$), deep red ($^3P_0 \rightarrow {}^3F_4$), orange ($^3P_0 \rightarrow {}^3H_6$), green ($^3P_1 \rightarrow {}^3H_5$), and blue ($^3P_0 \rightarrow {}^3H_4$) spectral regions have been demonstrated in tungstate [6], vanadate phosphors [8], molybdate [3], fluoride crystals [1,10], etc. Also, two dominant transitions from the fluorescent $^3P_0$ level of Pr^{3+} to the lower $^3H_6$ and $^3H_4$ states can be mixed to give out white light for application to white LEDs [11]. Presently, the rapid development of blue GaN laser diode operating around 450 nm, which can be used to directly pump the $^3P_{0,1,2}$ emitting levels of the Pr^{3+} ions, promotes the investigation of visible lasers of Pr^{3+} ion [3,10]. Actually, efficient continuous-wave green, orange, red and near-infrared lasers have been achieved in Pr-doped fluoride scheelite crystals at room-temperature as pumped by GaN laser diode, and the best results were obtained with the maximum output power 208 mW and the highest slope efficiency 59% [12]. The perspectives for the visible lasers are linked to the development of a new generation of colour displays, new data storage techniques, holographic techniques and also in medical treatments, etc.

The garnet crystals with the chemical formula $A_3B_2'B_3''O_{12}$ and space group *Ia3d* have attracted much attention for several decades. For instance, rare-earth ions doped GGG ($Gd_3Ga_5O_{12}$) crystals have been widely studied due to their excellent lasing properties, e.g. Nd:GGG [13], Er:GGG [14], Tm:GGG [15] and Dy:GGG [16] crystals. Also owing to the large heat capacity, it has been chosen as high-power solid heat capacity laser host. GGG crystal belongs to cubic system with the space group of $O_h{}^{10}$-*Ia3d*. The cell parameters are as follows: $a = 12.38$ Å, $Z = 8$ [17]. The melting point is 1725 °C and density is 7.09 g/cm^3 [18].

The combination of Pr^{3+} ions with this laser host is a promising media for visible solid-state device. There have been many reports on Pr^{3+}-doped GGG crystal, thin film or nanocrystalline [19–26], among which the topics involved crystal field analyses, cross-relaxation and energy transfer upconversion processes discussion, structural, luminescence properties investigation, etc. However, to our best knowledge, the Judd–Ofelt (J-O) theory [27,28] as one widely used and effective spectral analysis tool has not been used on Pr:GGG crystal till now. In this work, on the basis of the room-temperature measured absorption spectrum, fluorescence spectra and decay curves, the spectroscopic parameters of the Pr:GGG single crystal are obtained by using the standard and modified J-O theory, also the fluorescence properties of Pr:GGG with emphasis

* Corresponding author. Tel.: +86 591 8371 1368; fax: +86 591 8371 4946.
E-mail address: tcy@fjirsm.ac.cn (C. Tu).

0925-8388/$ – see front matter © 2010 Elsevier B.V. All rights reserved.
doi:10.1016/j.jallcom.2010.04.140

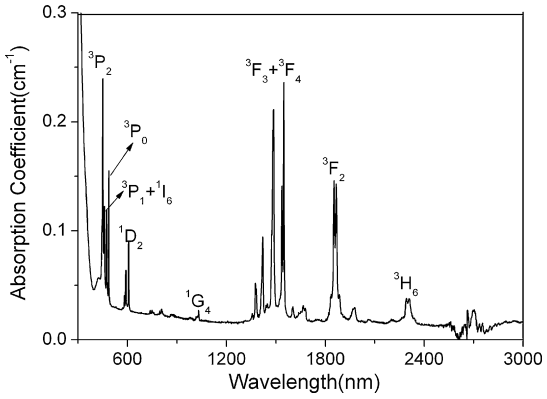

Fig. 1. Room-temperature absorption spectrum of Pr^{3+}:GGG crystal.

on $^3P_0$ and $^1D_2$ levels are analyzed and compared with referred results.

2. Experimental procedures

The 1.0 at% Pr^{3+}-doped GGG single crystal was grown by the Czochralski technique. The growth procedure was similar to that of Er:GGG described in our previous publication [29]. The concentration of praseodymium ions in the crystal was measured to be 0.268 wt% by the inductively coupled plasma-atomic emission spectrometry (ICP–AES) method and the corresponding Pr^{3+} concentration is 8.12×10^{19} ions/cm^3. The segregation coefficient K of Pr^{3+} ions in the GGG crystal can be estimated by:

$$K = \frac{C_{\text{cryst}}}{C_{\text{melt}}} \tag{1}$$

where C_{cryst} and C_{melt} are the Pr^{3+} concentrations in the grown crystal and the initial melt, respectively. Here, the segregation coefficient of Pr^{3+} in the GGG crystal was calculated to be 0.64.

The sample used for spectroscopic measurements was optically polished to flat and parallel faces. The thickness of the sample was measured to be 1.0 mm. Room-temperature absorption spectrum of this crystal was recorded by a PerkinElmer UV–vis–NIR spectrometer (Lambda-900). The fluorescence spectra and the decay curves were recorded at room-temperature by using an Edinburgh Instruments spectrophotometer (FLS920).

3. Results and discussion

3.1. Absorption spectroscopy and Judd–Ofelt analysis

The room-temperature absorption spectrum of Pr^{3+}:GGG is presented in Fig. 1. The terminal levels of the corresponding transitions from the $^3H_4$ ground state have been assigned by comparing the spectrum with previous data [30] and marked in Fig. 1. As seen from the spectrum, Pr^{3+}:GGG crystal shows strong absorption in the two bands with peaks at 450 nm and 590 nm, which can be pumped by Xenon lamp effectively.

For several decades, the Judd–Ofelt (J-O) [27,28] theory has been widely used to analyze the spectroscopic properties of rare-earth ions doped host materials. For Pr^{3+} ions, the magnetic dipole transitions are not taken into account in the J-O calculations owing to their slight contributions to the line strengths, so only the electric dipole transitions are considered. According to standard J-O theory, the measured line strength $S_{\text{meas}}(J \rightarrow J')$ can be calculated by using the following formula:

$$S_{\text{meas}}(J \rightarrow J') = \frac{3ch(2J+1)}{8\pi^3 N_0 \lambda e^2} \frac{9n}{(n^2+2)^2} \Gamma(\bar{\lambda}) \tag{2}$$

where N_0 is the Pr^{3+} concentration in the crystal (unit: ion/cm^3), $\bar{\lambda}$ is the mean wavelength of the absorption band, c is the vacuum speed of light, e is the electron charge, h is Planck's constant, J is the total angular momentum of the ground state ($J = 4$ in Pr^{3+}), n is the refractive index which can be calculated from the Sellmeier dispersion equation [31]:

$$n^2(\lambda) = 1 + \frac{2.7382\lambda^2}{\lambda^2 - (132.476)^2} \tag{3}$$

and $\Gamma(\bar{\lambda})$ is the integrated absorption coefficient for each absorption band which can be calculated by:

$$\Gamma(\bar{\lambda}) = \frac{\int D(\lambda)d\lambda}{L \log e} = \frac{\int D(\lambda)d\lambda}{0.4343L} \tag{4}$$

where L is the sample thickness, $D(\lambda)d\lambda$ is the measured optical density as a function of wavelength.

Then the measured line strengths were used to obtain J-O intensity parameters Ω_t ($t = 2$, 4, and 6) by fitting the following set of equations:

$$S_{\text{calc}}(J \rightarrow J') = \Omega_2 U^{(2)}_{JJ'_n} + \Omega_4 U^{(4)}_{JJ'_n} + \Omega_6 U^{(6)}_{JJ'_n} \tag{5}$$

$$U^{(t)}_{JJ'} = \left| < f^N \Psi J \left\| U^{(t)} \right\| f^N \Psi J' > \right|^2 \tag{6}$$

where $U^{(t)}_{JJ'}$ ($t = 2$, 4, 6) are the reduced matrix elements of tensor operators, given in Ref. [32]. When two absorption manifolds overlapped, the squared matrix element was taken to be the sum of the corresponding squared matrix elements. Combining the Eqs. (5) and (6) with the measured line strengths, the effective Judd–Ofelt intensity parameters for Pr:GGG were obtained. The root mean square (rms) deviation between the experimental and calculated line strengths was obtained by:

$$\text{rms}\Delta S = \sqrt{\sum_{i=1}^{N} \frac{(S_{\text{meas}} - S_{\text{calc}})^2}{(N-3)}} \tag{7}$$

where N is the number of absorption bands.

After a least-square fitting of S_{meas} to S_{calc}, the three J-O intensity parameters Ω_2, Ω_4 and Ω_6 were obtained to be -1.20×10^{-20}, 5.72×10^{-20} and 3.86×10^{-20} cm^2, respectively. And the value of the relative error of the fitting given by rmsΔS/rms$S$ was calculated to be 2.377. The experimental and calculated line strengths are listed in Table 1, among which the values of the $^3H_4 \rightarrow {}^3P_2$ transition of Pr^{3+} in GGG crystal are 4.99×10^{-20} and 0.73×10^{-20} cm^2, respectively. Here appeared a negative value for the parameter Ω_2, which is meaningless in physics, and large deviation between calculated and experimental absorption line strengths for the Pr:GGG crystal by using the standard J-O theory. These were also encountered in other Pr^{3+}-doped materials [33–35]. The abnormal results are usually explained by the smaller gap between barycenters of the $4f^2$ ground and $4f^1 5d^1$ excited configuration of Pr^{3+} than those of other lanthanide ions, which tends to make the absorption transitions to high-lying $4f^2$ states stronger than the prediction of the J-O theory [30]. In order to overcome the problems, it is customary to simply exclude the value of the hypersensitive transition $^3H_4 \rightarrow {}^3P_2$, in which $^3P_2$ is the most high-lying $4f^2$ state of Pr^{3+} ions (as identified in Fig. 1). In the fitting procedure large discrepancy between the calculated and experimental line strengths is owing to this transition [35,36]. For the Pr:GGG crystal, J-O intensity parameters were then recalculated after excluding the relevant values of $^3H_4 \rightarrow {}^3P_2$ transition in the fitting procedure. Then we found decreased value of rms error and minor changes in the Ω_t setting, the three J-O intensity parameters were obtained to be -0.92×10^{-20} cm^2, 5.73×10^{-20} cm^2 and 3.50×10^{-20} cm^2, respectively, but Ω_2 still be negative. The obtained results are also shown in Table 1.

Modified J-O theory as one method to improve the reliability of the J-O parameters has been proposed by Dunina et al [36]. This theory improved calculated line strengths with an additional intro-

Table 1
Experimental and calculated line strengths of Pr^{3+}:GGG crystal by using the standard and modified J-O theory (S is in units of 10^{-20} cm^2).

Excited states	$\bar{\lambda}$ (nm)	$\Gamma(\bar{\lambda})$ (nm/cm)	The standard J-O theory				The modified J-O theory			
			With $^3H_4 \rightarrow {}^3P_2$		Without $^3H_4 \rightarrow {}^3P_2$		With $^3H_4 \rightarrow {}^3P_2$		Without $^3H_4 \rightarrow {}^3P_2$	
			S_{meas}	S_{calc}	S_{meas}	S_{calc}	S_{meas}	S_{calc}	S_{meas}	S_{calc}
$^3H_6$	2292	21.59	0.576	3.38	0.576	3.192	0.749	1.681	0.749	1.271
$^3F_2$	1853	79.74	2.611	2.147	2.611	2.254	2.872	2.695	2.872	2.757
$^3F_3 + {}^3F_4$	1548	194.5	7.622	6.736	7.622	6.336	4.073	3.389	4.073	3.706
$^1G_4$	1031	1.53	0.089	0.142	0.089	0.133	0.123	0.093	0.123	0.114
$^1D_2$	607	12.44	1.223	0.295	1.223	0.277	2.449	2.137	2.449	2.246
$^3P_0$	487	7.97	0.952	0.988	0.952	0.991	2.332	2.136	2.332	2.286
$^3P_1 + {}^1I_6$	473	6.0	0.738	1.353	0.738	1.35	1.287	1.657	1.287	1.503
$^3P_2$	450	38.92	4.991	0.730	–	–	5.518	4.644	–	–
rms error			2.377	1.573	1.598	0.661				

duced parameter. The modified line strength formula is expressed as

$$S_{calc} = S_{calc}(standard)\left[1 + \frac{E_i - 2E_f^0}{E_{5d} - E_f^0}\right] \quad (8)$$

where the standard line strength is defined in Eq. (5), E_i is the energy of transition, E_{5d} is the energy of the lowest $4f5d$ state, and E_f^0 is the average energy over the $4f^2$ states. The values of E_f^0 and E_{5d} are 10,000 and 60,000 cm^{-1}, respectively [34]. By applying the modified J-O theory and including or excluding the $^3H_4 \rightarrow {}^3P_2$ transition in the calculation, we got the experimental and calculated line strengths for Pr^{3+}:GGG crystal, as given in Table 1. Table 2 shows the J-O intensity parameters for Pr^{3+} ion in GGG crystal and other crystal hosts. As seen from the tables, the values of line strengths and J-O parameters are reasonable by using the modified JO theory without considering the $^3H_4 \rightarrow {}^3P_2$ transition. Also, we can find that Pr:GGG has relatively smaller values as compared with other two kinds of Pr^{3+} doped garnet laser crystals. In the following analysis, the J-O parameters determined by the modified J-O theory without the $^3H_4 \rightarrow {}^3P_2$ transition are adopted.

The radiative transition probabilities of the transitions from an excited manifold J to a lower manifold J' can be calculated from the J-O parameters by:

$$A(J \rightarrow J') = \frac{64\pi^4 e^2}{3h(2J+1)\bar{\lambda}^3}\frac{n(n^2+2)^2}{9} \times \sum_{t=2,4,6} \Omega_t \left|\left\langle (S,L)J \left\| U^{(t)} \right\| (S',L')J' \right\rangle\right|^2 \times \left[1 + \frac{E_i - 2E_f^0}{E_{5d} - E_f^0}\right] \quad (9)$$

The emission transition matrix elements for Pr^{3+} have been tabulated in Ref. [40]. The radiative branching ratio is expressed as:

$$\beta_{JJ'} = \frac{A(J \rightarrow J')}{\sum_{J'} A(J \rightarrow J')} \quad (10)$$

And the radiative lifetime is

$$\tau_{Rad} = \frac{1}{\sum_{J'} A(J \rightarrow J')} \quad (11)$$

According to the above equations and the relevant data, the radiative transition probabilities, branching ratios and the radiative lifetimes of Pr^{3+} in GGG crystal for different transition levels can be obtained, which are given in Table 3.

3.2. Fluorescence spectroscopy and stimulated emission cross-sections

The room-temperature emission spectrum of Pr^{3+}:GGG in the visible region excited by 450 nm pumping is shown in Fig. 2. Seven emission bands with peak at 487, 531, 561, 617, 658, 712, 740 nm can be observed, and the emissions mainly origin from the metastable $^3P_0$ manifolds. The two most intensive emission located around 617 nm and 658 nm are assigned to the transitions $^3P_0 \rightarrow {}^3H_6$ and $^3P_0 \rightarrow {}^3F_2$, respectively.

The room-temperature fluorescence spectra in the spectral region 600–1250 nm of this crystal excited by 590 nm pumping are shown in Fig. 3. The are mainly two emission bands between 600 and 800 nm with peaks 607 and 634 nm, and two main emission bands are located around 825 and 1062 nm in the region of 800–1200 nm; all the fluorescence emission bands are mainly assigned to the transitions from the $^1D_2$ manifold, as listed in Table 4.

The emission cross-sections is an important parameter influencing the potential laser performance. The stimulated emission cross-sections can be estimated from the room-temperature fluorescence spectra by using the Füchtbauer–Ladenburg (F-L) formula [41]:

$$\sigma_{em}(\lambda) = \frac{\lambda^5 A(J \rightarrow J')I(\lambda)}{8\pi c n^2 \int \lambda I(\lambda) d\lambda} \quad (12)$$

where $I(\lambda)$ is the experimental emission intensity as a function of the wavelength λ. With the present data we can estimate the emission cross-sections of the transitions from $^3P_0$ and $^1D_2$ manifold. Table 4 shows the emission peak wavelengths and cross-sections of several main transitions for Pr^{3+}:GGG crystal. It can be found that the peak emission cross-sections of the $^3P_0 \rightarrow {}^3F_2$ as red laser

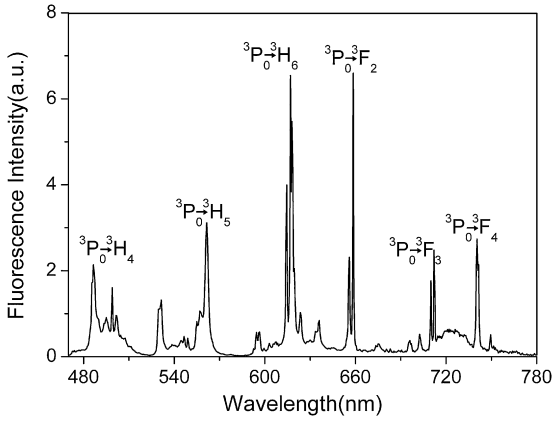

Fig. 2. Visible fluorescence spectrum of Pr^{3+}:GGG crystal excited by 450 nm pumping.

Table 2
The J-O intensity parameters of Pr^{3+}-doped crystals.

Material	$\Omega_2(10^{-20}\,cm^2)$	$\Omega_4(10^{-20}\,cm^2)$	$\Omega_6(10^{-20}\,cm^2)$	Ref.
YAG	0	12.2	8.27	[38]
$YAlO_3$	2	6	7	[39]
LaF_3	0.12 ± 0.91	1.77 ± 0.81	4.78 ± 0.52	[40]
GGG	0.76	4.84	1.02	This work

Table 3
Calculated radiative transition rates, branching ratios and radiative lifetimes for different transition levels of Pr^{3+}: GGG crystal.

Transition		Wavelength (nm)	$A\,(s^{-1})$	β	$\tau_r\,(\mu s)$
$^3P_0 \rightarrow$	$^1D_2$	2594	2.951	2.087E−4	71
	$^1G_4$	9248	0.74	5.23E−5	
	$^3F_4$	740	2438	0.172	
	$^3F_3$	712	0	0	
	$^3F_2$	658	847.81	0.06	
	$^3H_6$	617	685.16	0.048	
	$^3H_5$	531	0	0	
	$^3H_4$	487	10,170	0.719	
$^1D_2 \rightarrow$	$^1G_4$	1439	362.5	0.046	128
	$^3F_4$	1062	374.2	0.048	
	$^3F_3$	937	540.73	0.069	
	$^3H_6$	825	1532	0.196	
	$^3H_5$	634	2697.8	0.345	
	$^3H_4$	607	2311	0.296	

channel is $3.27 \times 10^{-20}\,cm^2$, and this band has the largest emission cross-sections among all the emission bands of Pr:GGG crystal. While the emission cross-sections of 1.25% Pr^{3+}-doped $LiLuF_4$ crystal at 640.2 nm is $2.2 \times 10^{-19}\,cm^2$, in which a red laser has been achieved [10]. As we conceive, if Ce^{3+} or other ions is co-doped into Pr:GGG crystal, direct and trap mediated capture and recombination of holes and electrons via Pr^{3+} and Ce^{3+} or other ions might provide the larger photon production in GGG crystals, and help to increase the emission intensity and cross-sections of visible bands.

3.3. Fluorescence lifetimes and quantum efficiency

In order to get better understanding of fluorescence dynamics, we measured the decay curves of several transitions originating from $^3P_0$ and $^1D_2$ levels. Fig. 4 shows the luminescence decay curves recorded at 617 nm excited by 450 nm. It was found that the decay curve is single exponential, which means that no energy transfer processes involving the $^3P_0$ level are present in this system. And the lifetime $^3P_0 \rightarrow {}^3H_6$ transition was fitted to be 21.0 μs, which is close to 1 mol% Pr:GGG nanocrystalline: 18 μs [25]. The experimental lifetime value of the $^3P_0$ level can be compared to those of 1% Pr^{3+}:YAG: 8.4 μs [42], of 1% Pr^{3+}:YAP: 9.2 μs [43] and of 0.01% Pr^{3+}:LaF_3: 47 μs [44]. By following the calculation equation of quantum efficiency $\eta = \tau_f/\tau_r$, we can obtain the quantum efficiencies of $^3P_0 \rightarrow {}^3H_6$ transitions to be 29.6%, which can be compared with the quantum efficiencies of 1% Pr:YAG (82.3% [37]) and 1% YAP (70% [43]). The relatively low quantum efficiency of this transition might be due to the static perturbations of the crystal fields led by Gd^{3+} in octahedral a sites being a non-stoichiometric defect [21].

Table 4
The stimulated emission cross-sections of main transitions for Pr^{3+}:GGG crystal.

Transition	Wavelength (nm)	$\sigma_e\,(10^{-20}\,cm^2)$
$^3P_0 \rightarrow {}^3H_4$	487	0.11
$^3P_0 \rightarrow {}^3H_6$	617	0.76
$^3P_0 \rightarrow {}^3F_2$	658	3.27
$^3P_0 \rightarrow {}^3F_4$	740	2.57
$^1D_2 \rightarrow {}^3H_4$	607	2.52
$^1D_2 \rightarrow {}^3H_5$	634	0.64
$^1D_2 \rightarrow {}^3H_6$	825	1.24
$^1D_2 \rightarrow {}^3F_4$	1062	1.65

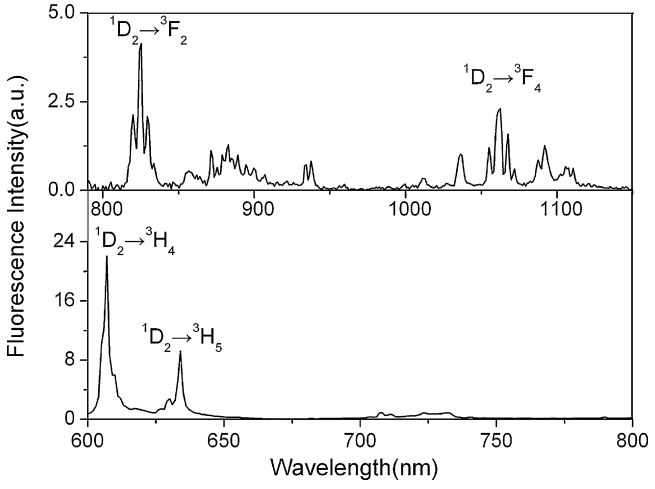

Fig. 3. Visible and infrared fluorescence spectra of Pr^{3+}:GGG crystal excited by 590 nm pumping.

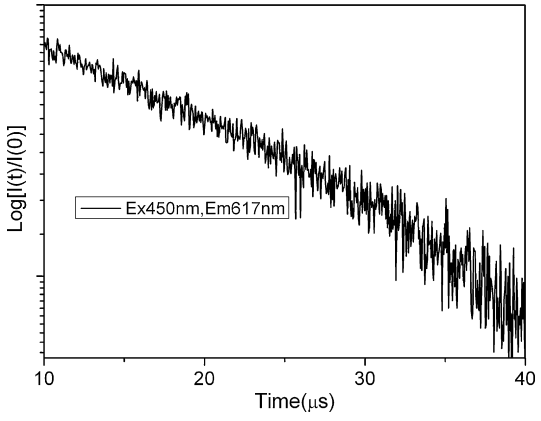

Fig. 4. Room-temperature luminescence decay curve at 617 nm excited by 450 nm pumping.

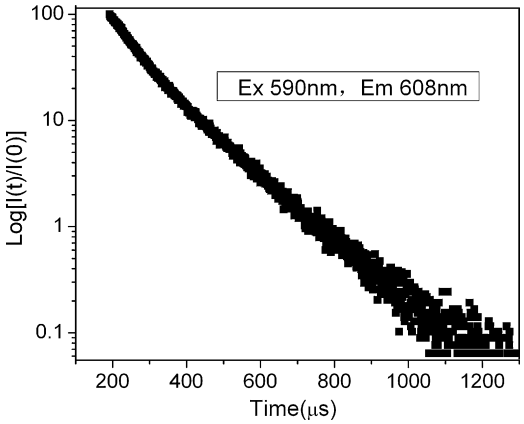

Fig. 5. Room-temperature luminescence decay curve at 608 nm excited by 590 nm pumping.

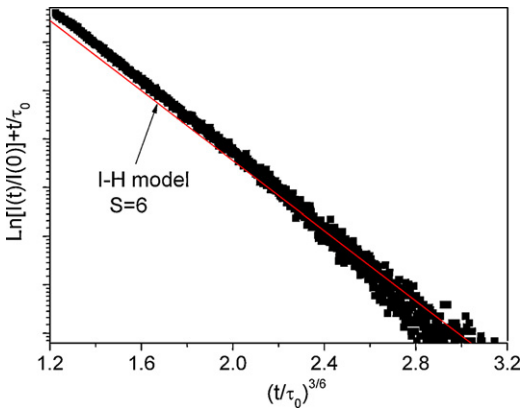

Fig. 6. The fitting fluorescence decay curve for the $^1D_2 \rightarrow {}^3H_4$ transition obtained using the Inokuti-Hirayama model with $S = 6$.

As demonstrated in Fig. 5, the luminescence decay curve of the $^1D_2 \rightarrow {}^3H_4$ transition at the wavelength of 608 nm excited by 590 nm pumping is not singly exponential, but could be described as two exponentials, among which the lifetime of τ_1 and τ_2 components are estimated to be 63.5 and 144.6 μs, respectively. And the lifetime the $^1D_2$ manifold is estimated to be 118.4 μs by using $\tau = (B_1\tau_1^2 + B_2\tau_2^2)/(B_1\tau_1 + B_2\tau_2)$ [29], which is much longer than that of $^3P_0$ level. The experimental lifetime value of the $^1D_2$ level can be compared to that of 1 mol%Pr:GGG nanocrystalline: 110μs [25], 0.5% Pr^{3+}:YAG: 110μs [45] and of 1% Pr^{3+}:YAP: 28μs [43]. It is interesting to point that at 4 K the decay $^1D_2 \rightarrow {}^3H_4$ profile of Pr:GGG is exponential with a lifetime of 260 μs [23], as in contrast with the above results of this job. The quantum efficiency of the $^1D_2 \rightarrow {}^3H_4$ transition for Pr:GGG crystal is calculated to be 92.5%, which is higher than that of 1% Pr:YAG: 90% [37]. Furthermore, the peak emission cross-sections of the $^1D_2 \rightarrow {}^3H_4$ as yellow laser channel is 2.52×10^{-20} cm^2 as seen from Table 4; combing the large emission cross-sections value with the high quantum efficiency, it might be possible to realize yellow laser gain in Pr:GGG crystal.

The non-exponential character of the excited $^1D_2$ decay could be explained by a nearly resonant cross-relaxation process between the Pr ions in excited state and the ground state, the likely path is $^1D_2 + {}^3H_4 \rightarrow {}^1G_4 + {}^3F_4$ [46]; this phenomenon was observed in Pr:GGG nanocrystalline samples too [25]. Here, the Inokuti–Hirayama theory [47] was used to understand the decay curve:

$$I(t) = I(0)\exp\left[-\frac{t}{\tau_0} - \Gamma\left(1-\frac{3}{S}\right)\frac{N_0}{C_0}\left(\frac{t}{\tau_0}\right)^{3/S}\right] \quad (13)$$

where τ_0 is the fluorescence lifetime in absence of the energy transfer, N_0 is the Pr^{3+} ion concentration in cm^{-3}, $C_0 = 3/4\pi R_c^3$, is the critical concentration and $\Gamma(x)$ is the gamma function of x, and $S = 6$, 8 or 10 corresponds to the transfer mechanism of electric dipole–dipole, dipole–quadrupole or quadrupole–quadrupole character, respectively. Then, the fluorescence decay curve of the $^1D_2 \rightarrow {}^3H_4$ transition is plotted as $\ln[I(t)/I(0)] + t/\tau_0$ versus $(t/\tau_0)^{3/S}$ and linear fitting is made to get the best value of S, as shown in Fig. 6. During the fitting process, the τ_0 value at low Pr^{3+} concentration was used as an additional free parameter. The best fitting was obtained when $S = 6$, $\tau_0 = 128$ μs. It demonstrates that the cross-relaxation energy transfer caused by the electric dipole-dipole transfer mechanism is responsible for the non-exponential decaying behavior of the $^1D_2$ manifold for Pr^{3+} ions in GGG, and for the shorter fluorescence lifetime than the radiative lifetime.

4. Conclusions

The absorption spectrum of Pr^{3+}-doped GGG single crystal was analyzed by the standard and modified J-O theories, and the best fitting results were obtained by the modified J-O theory without the $^3H_4 \rightarrow {}^3P_2$ transition. Three J-O intensity parameters were obtained to be: $\Omega_2 = 0.76 \times 10^{-20}$ cm^2, $\Omega_4 = 4.84 \times 10^{-20}$ cm^2 and $\Omega_6 = 1.02 \times 10^{-20}$ cm^2. The stimulated emission cross-sections of some typical fluorescence transitions were estimated by using F-L equation. The fluorescence lifetimes of $^3P_0$ and $^1D_2$ levels were determined and the quantum efficiencies were estimated. Results of this work conclude that $^3P_0$ and $^1D_2$ manifolds of the Pr^{3+}-doped GGG crystal are suitable as the upper laser levels, and Pr^{3+}:GGG crystal may be a potential candidate for visible solid-state laser medium.

Acknowledgements

This work was supported by the Science & Technology Plan Projects of Fujian Province of China (2007H0037), the Great Projects of FJIRSM (SZD08001-2; SZD09001), the Fund of Key Laboratory of Optoelectronic Materials Chemistry and Physics of CAS (no. 2008DP173016), and the National Nature Science Foundation of China (no. 50902129).

References

[1] S. Khiari, M. Velazquez, R. Moncorgé, J.L. Doualan, P. Camy, A. Ferrier, M. Diaf, J. Alloys Compd. 451 (2008) 128.
[2] L. Macalik, M. Mączka, J. Hanuza, P. Godlewska, P. Solarz, W. Ryba-Romanowski, A.A. Kaminskii, J. Alloys Compd. 451 (2008) 232.
[3] W. Guo, Y. Lin, X. Gong, Y. Chen, Z. Luo, Y. Huang, Appl. Phys. B 94 (2009) 155.
[4] P.J. Dereń, R. Pązik, W. Stręk, Ph. Boutinaud, R. Mahiou, J. Alloys Compd. 451 (2008) 595.
[5] E. Brown, U. Hömmerich, T. Yamada, H. Yamane, J.M. Zavada, J. Alloys Compd. 488 (2009) 628.
[6] J. Chen, X. Gong, Y. Lin, Y. Chen, Z. Luo, Y. Huang, J. Alloys Compd. 492 (2010) 667.
[7] S. Cao, Y. Ma, C. Quan, W. Zhu, K. Yang, W. Yin, G. Zheng, M. Wu, Z. Sun, J. Alloys Compd. 487 (2009) 346.
[8] X. Yang, X. Yu, H. Yang, Y. Guo, Y. Zhou, J. Alloys Compd. 479 (2009) 307.
[9] M. El Okr, M. Farouk, M. El-Sherbiny, M.A.K. El-Fayoumi, M.G. Brik, J. Alloys Compd. 490 (2010) 184.
[10] F. Cornacchia, A. Richter, E. Heumann, G. Huber, D. Parisi, M. Tonelli, Opt. Express. 15 (2007) 992.
[11] Xiaoding Qi, Chieh-Min Liu, Chung-Chiang Kuo, J. Alloys Compd. 492 (2010) L61.
[12] F. Cornacchia, A. Di Lieto, M. Tonelli1, A. Richter, E. Heumann, G. Huber, Opt. Express. 16 (2008) 15932.
[13] Z.B. Wang, Q.L. Zhang, D.L. Sun, S.T. Yin, J. Rare Earthroom-temperatures 25 (2007) 244.
[14] B.J. Dinerman, P.F. Moulton, Opt. Lett. 19 (1994) 1143.
[15] H. Zhou, X. Ma, G. Chen, W. Lv, Y. Wang, Z. You, J. Li, Z. Zhu, C. Tu, J. Alloys Compd. 475 (2009) 555.

[16] Y. Wang, Z. You, J. Li, Z. Zhu, C. Tu, J. Phys. D: Appl. Phys. 43 (2010) 075402.
[17] G.J. Kintz, L. Esterowitz, R. Allen, Electron. Lett. 23 (1987) 616.
[18] D.J. Tao, G.X. Zhu, S.T. Yin, Chin. J. Quantum Electron. 20 (2003) 550.
[19] E. Antic-Fidancev, Eur. J. Solid State Inorg. Chem. 28 (1991) 81.
[20] E. Antic-Fidancev, J. Holsa, J.C. Krupa, M. Lemaitre-Blaise, P. Porcher, J. Phys. Condens. Matter 4 (1992) 8321.
[21] A. Lupei, H. Gross, P. Reiche, J. Phys. Condens. Matter 7 (1995) 5701.
[22] J. Lancok, C. Garapon, M. Jelinek, J. Mugnier, R. Brenier, Appl. Phys. A 81 (2005) 1477.
[23] J.A. Capobianco, N. Raspa, A. Monteil, M. Malinowski, J. Phys. Condens. Matter 5 (1993) 6083.
[24] M. Malinowski, R. Piramidowicz, J. Sarnecki, W. Wolinski, J. Phys. Condens. Matter 10 (1998) 1909.
[25] R. Naccache, F. Vetrone, A. Speghini, M. Bettinelli, J.A. Capobianco, J. Phys. Chem. C 112 (2008) 7750.
[26] N. Raspa, PhD Thesis; Concordia University, Montreal, Canada, 1992.
[27] B.R. Judd, Phys. Rev. 127 (1963) 750.
[28] G.S. Ofel, J. Chem. Phys. 37 (1962) 511.
[29] Y. Wang, Z. You, J. Li, Z. Zhu, E. Ma, C. Tu, J. Phys. D: Appl. Phys. 42 (2009) 215406.
[30] A.A. Kaminskii, Laser Crystal: Their Physics and Properties, second ed., Springer-Verlag, Berlin, 1990.
[31] D.K. Sardar, W.M. Bradley, M.R. Kokta, J. Appl. Phys. 93 (2003) 2602.
[32] W.T. Carnall, P.R. Fields, K. Rajnak, J. Chem. Phys. 49 (1968) 4424.
[33] R.S. Quimby, W.J. Miniscalco, J. Appl. Phys. 75 (1994) 613.
[34] P. Goldner, F. Auzel, J. Appl. Phys. 79 (1996) 7972.
[35] H. Wang, G. Jia, F. Yang, Y. Wei, C. Tu, Z. You, Y. Wang, Z. Zhu, J. Li, J. Appl. Phys. 100 (2006) 113117-1.
[36] E.B. Dunina, A.A. Kaminskii, A.A. Kornienko, K. Kurbanov, K.K. Pukhov, Sov. Phys. Solid State 32 (1990) 290.
[37] M. Malinowski, R. Wolski, W. Wolinski, Solid State Commun. 74 (1990) 17.
[38] M.J. Weber, T.E. Varitimos, B.H. Matsiner, Phys. Rev. B 8 (1973) 47.
[39] W.F. Krupke, Phys. Rev. 145 (1966) 325.
[40] A. Kaminskii, E. Belokoneva, B. Mill, S. Sarkisov, K. Kurbanov, Physica Status Solidi A 97 (1986) 279.
[41] B.M. Walsh, N.P. Barnes, B. Di Bartolo, J. Appl. Phys. 83 (1998) 2772.
[42] M. Malinowski, W. Wolinski, R. Wolski, W. Strek, J. Lumin. 48 (1991) 235.
[43] G. Ozen, O. Forte, B. Di Bartolo, J.M. Collins, J. Lumin. 125 (2007) 223.
[44] M.J. Weber, J. Chem. Phys. 48 (1968) 4774.
[45] G. Ozen, O. Forte, B. Di Bartolo, J. Appl. Phys. 97 (2005) 013510.
[46] X. Lu, Z. You, J. Li, Z. Zhu, G. Jia, B. Wu, C. Tu, Appl. Phys. B 85 (2006) 585.
[47] M. Inokuti, F. Hirayama, J. Chem. Phys. 43 (1965) 1978.